Removal and Recovery of Heavy Metal Ions by Two-dimensional MoS_2 Nanosheets: Performance and Mechanisms

Research article

Revision submitted to

Environmental Science & Technology

June 3, 2018

Zhongying Wang[1], Alison Sim[1], Jeffrey J. Urban[2], Baoxia Mi[1*]

[1]Department of Civil and Environmental Engineering, University of California, Berkeley, California 94720, United States

[2]The Molecular Foundry, Lawrence Berkeley National Laboratory, Berkeley, California 94720, United States

*The author to whom correspondence should be addressed.

e-mail: mib@berkeley.edu; tel.: +1-510-664-7446, fax: +1-510-643-5264

Abstract

We investigated the removal of heavy metals from water by two-dimensional MoS_2 nanosheets suspended in aqueous solution, and restacked as thin film membranes, respectively. From these studies we elucidated a new heavy metal ion removal mechanism that involves a reduction–oxidation (redox) reaction between heavy metal ions and MoS_2 nanosheets. Ag^+ was used as a model species and MoS_2 nanosheets were prepared via chemical exfoliation of bulk powder. We found that the Ag^+ removal capacity of suspended MoS_2 nanosheets was as high as ~4000 mg/g and adsorption accounted for less than 20% of removal, suggesting the reduction of Ag^+ to metallic silver as a dominant removal mechanism. Furthermore, we demonstrated that MoS_2 membranes were able to retain a similar high removal capacity, and attribute this capability to the formation of a conductive, permeable multilayer MoS_2 structure, which enables a corrosion-type reaction involving electron transfer from a MoS_2 site inside the membrane (anode) to another site on membrane surface (cathode) where heavy metal ions are reduced to metallic particles. The membrane surface remains active to efficiently recover metallic particles, because the primary oxidation products are soluble, non-toxic molybdate and sulfur species, which do not form an insulating oxide layer to passivate the membrane surface. Therefore, MoS_2 membranes can be used effectively to remove and recover precious heavy metals from wastewater.

TOC/Abstract Art

42 **INTRODUCTION**

43 The presence of toxic waterborne pollutants, particularly heavy metal ions (e.g., Ag^{+}, Hg^{2+}, Pb^{2+})
44 in wastewater and natural water resources, poses a pressing challenge to public health[1] and hence
45 calls for effective treatment technologies to reduce such contents to trace levels (ppb).[2] The
46 technologies for selective removal of heavy metal ions, due to their small size, positive charge,
47 and similarity to other ions (e.g., Ca^{2+}, Na^{+}) abundant in water, are often different from those for
48 other contaminants (e.g., organics).[2] Compared with technologies such as precipitation,
49 coagulation, and membrane separation, adsorption is favored due to its low cost, ease of operation,
50 and recyclability. Typical adsorbent materials, including activated carbon,[3] clay,[4] nanocellulose,[5]
51 graphene-based material,[6] and biomass,[7] are usually cost-effective and have high surface areas.
52 However, the selectivity of these absorbents towards target contaminants is often poor because of
53 competitive adsorption and thus compromised adsorption performance in treating waters with
54 complex components.[8,9] Therefore, strong specific interactions between target contaminants and
55 adsorbents are desired in order to simultaneously achieve high capacity and good selectivity.[10,11]
56 For the selective removal of heavy metals, sulfur-containing or sulfur-functionalized materials
57 have been studied and used extensively as superior adsorbents due to the high affinity of sulfur to
58 heavy metal ions *via* Lewis soft-soft interactions.[10-13]

59 As a representative member of transition metal dichalcogenides (TMDs), the newly
60 emerging two-dimensional (2D) layered molybdenum disulfide (MoS_2) has demonstrated great
61 promise for numerous environmental applications,[14] particularly used as an adsorbent material to
62 remove heavy metal pollutants due to its sulfur-rich surface.[15-20] Each MoS_2 monolayer consists
63 of covalently bonded atomic trilayers of sulfur–molybdenum–sulfur, and multiple monolayers are
64 stacked via weak van der Waals force to form a bulk crystal. As a naturally occurring mineral,
65 however, bulk MoS_2 is rarely used as an adsorbent because of the small free spacing (0.3 nm)
66 between its neighboring layers, which limits the access of ionic species to interior sulfur atoms.[18]
67 Thanks to various synthetic routes developed in the past years, 2D MoS_2 nanosheets can be either
68 exfoliated from bulk material or synthesized using Mo/S precursors to expose sulfur atoms on both
69 sides of a MoS_2 nanosheet,[21-23] offering substantial accessible adsorption sites and hence ensuring
70 high removal capacity. For example, it has been reported that after the interlayer spacing between
71 MoS_2 nanosheets is widened to 0.94 nm, an extremely high mercury uptake capacity close to the

72 theoretically predicted level of 2506 mg/g can be achieved.[18] The mechanism for Hg^{2+} adsorption
73 has been associated with ion exchange between Hg^{2+} and cations (*e.g.*, H^+) on the MoS_2 surface.[18]
74 In addition, it has been demonstrated that Hg^{2+} can be adsorbed on MoS_2 surface in the form of
75 multilayers, where the adsorption of the first layer is attributed to the complexation of Hg^{2+} with
76 S atoms while the adsorption of subsequent layers mainly results from electrostatic interaction.[15]
77 Besides Hg^{2+}, other toxic heavy metal ions such as Pb(II),[24-26] Cr(VI),[27] Ni(II),[20] and Co(II) [28] can
78 also be satisfactorily adsorbed by 2D MoS_2 nanosheets.

79 Despite the promise of MoS_2 nanosheets as a highly efficient adsorbent, the effects of
80 MoS_2-M^{n+} interactions and key material properties (e.g., phase, surface area, charge, redox
81 potential) on the removal performance (e.g., heavy metal removal capacity) of MoS_2-based
82 materials remain largely unknown. Different synthetic routes may produce MoS_2 nanosheets with
83 distinct crystal configurations and physicochemical properties,[14,29] potentially leading to different
84 removal capacities. For instance, depending on atom-stacking configurations, synthetic MoS_2
85 nanosheets can be either in the metallic octahedral 1T phase or in the semiconducting trigonal
86 prismatic 2H phase.[29] Currently, the facile hydrothermal (or solvothermal) reaction is the most
87 employed procedure for assembling MoS_2 nanosheets to remove heavy metal ions.[17,18,20,24,25,28]
88 However, the effects of different percentages of 1T/2H phases in such MoS_2 products[23,30] on their
89 metal removal capability have not been studied. As the arguably most scalable method for
90 preparing monolayer MoS_2 nanosheets, the intercalation-induced interlayer expansion and
91 exfoliation produces the chemically exfoliated MoS_2 (ce-MoS_2) nanosheets,[21,31] which have
92 negatively charged surfaces with defects on their edges and basal planes,[32,33] providing additional
93 binding sites for adsorption. During the exfoliation process, MoS_2 is converted from 2H phase in
94 bulk material to 1T/2H mixture in final products.[21,29] So far, the heavy metal ion removal
95 performance and the corresponding mechanisms of ce-MoS_2 nanosheets have yet been studied.
96 Besides the application of 2D MoS_2 nanosheets in dispersed form, their potential use in the form
97 of layer-stacked thin film membrane[34,35] to remove and even recover precious metals from
98 wastewater has not been explored.

99 To address the above research needs, we systematically investigated in this study the heavy
100 metal ion removal performance of 2D ce-MoS_2 nanosheets dispersed in water and restacked as
101 thin film membrane, respectively, with an emphasis on the effects of MoS_2-M^{n+} interactions and

102 material properties on such performance. We also fundamentally elucidated the mechanisms
103 underlying the removal capacity, kinetics, and selectivity of such 2D materials as well as the
104 continuous removal and recovery capability of MoS_2 membranes.

105 MATERIALS AND METHODS

106 **Preparation of MoS_2 Nanosheets and Membranes.** The ce-MoS_2 dispersion was produced by
107 exfoliating the commercially available MoS_2 powder (Sigma-Aldrich, Saint Louis, MO) through
108 a well-established chemical exfoliation process,[21] which is briefly described here. Bulk MoS_2
109 powder was immersed in n-Butyllithium hexane solution for 2 days in an anaerobic condition to
110 enable Li intercalation, followed by reaction in deionized (DI) water to allow interlayer spacing
111 expansion and nanosheet exfoliation. The resulting suspension was subjected to dialysis (3.5K
112 MWCO Dialysis Tubing, Thermo Scientific, Saint Louis, MO) in DI water to remove all soluble
113 by-products. MoS_2 concentration of the suspension was determined by digestion in 2% HNO_3,
114 followed by measuring the concentration of soluble Mo species. MoS_2 nanosheets remained well-
115 dispersed in suspension during storage, and this suspension was directly diluted to desired
116 concentration for removal tests. To aid comparison with ce-MoS_2 about the phase effect,
117 ultrasonically exfoliated MoS_2 (ue-MoS_2) nanosheets were prepared with probe sonication in
118 sodium cholate solution using a liquid-phase exfoliation procedure from literature.[22] Excess
119 surfactant (sodium cholate) was removed by repeated centrifugation and redispersion with DI
120 water. Unlike ce-MoS_2 that often involves phase conversion during preparation, ue-MoS_2
121 nanosheets mostly remain as 2H-MoS_2 after exfoliation.[36] The sizes of produced MoS_2 nanosheets
122 were evaluated by atomic force microscopy (AFM, Bruker Dimension Icon) and high-resolution
123 transmission electron microscopy (HRTEM, JEOL 2100F). The layer-stacked MoS_2 membrane
124 was prepared by vacuum filtration of ce-MoS_2 dispersion through a poly(ether sulfone) (PES)
125 ultrafiltration substrate with a nominal pore size of 30 nm. Typically, 2 mL of ce-MoS_2 solution
126 (0.3 mg/mL) was needed to make a ~0.2-μm-thick membrane.

127 **Heavy Metal Uptake Experiments.** Removal of Ag^+ (as a model heavy metal ionic species) from
128 aqueous solution was studied by the batch method to evaluate the removal capacity, kinetics, and
129 selectivity of MoS_2 nanosheets. In a typical batch test, ce-MoS_2 suspension was added with silver
130 nitrate solution and then agitated at 120 rpm on a mechanical shaking table for 1 day. Then, all
131 particulates were removed using a syringe filter with a nominal pore size of 20 nm (Anotop 10

132 Plus, Whatman, Maidstone, UK), and the concentration of Ag^+ (as well as other ionic species) in
133 the filtrate solution was measured using inductively coupled plasma-optical emission spectroscopy
134 (ICP-OES, Agilent 720, Agilent Technologies, Santa Clara, CA). Buffer solutions (acetate buffers,
135 pH 3 and 4.5; MES buffer, pH 6) were used if necessary. To determine the equilibrium removal
136 capacity, ce-MoS_2 nanosheets were immersed in Ag^+ solution for 1 day to achieve the equilibrium
137 state of adsorption. Selectivity of Ag^+ removal was tested with $NaNO_3$ solutions at concentrations
138 of 0.001, 0.01, 0.1, and 1M, respectively. In selected experiments, an anaerobic condition was
139 created by continuously purging the entire system with nitrogen gas. For the experiments with
140 MoS_2 membranes, two setups were used: one for membrane directly soaked in metal-ion-
141 containing solution to recover metal, and the other for membrane installed in a membrane filtration
142 cell, where metal-ion-containing solution was filtered through the membrane under an external
143 pressure of 20 psi (1.4 bar). In each case, the concentrations of remaining metal ions and released
144 soluble Mo species were measured by ICP-OES.

145 **Characterization Techniques.** The morphology and elemental distribution were obtained by a
146 scanning electron microscopy (SEM, Phenom ProX, Netherlands) with an energy-dispersive
147 spectroscopy (EDS, INCA Energy EDS, Phenom ProX, Netherlands). The imaging and mapping
148 were performed using acceleration voltages of 10 kV and 15 kV, respectively. X-ray photoelectron
149 spectroscopy (XPS) analysis was carried out using a K-Alpha XPS spectrometer (Thermo
150 Scientific Ltd, East Grinstead, UK), and the atomic percentage of peaks was determined by a peak-
151 fitting analysis using a nonlinear Shirley-type background. Powder X-ray diffraction (XRD)
152 patterns were obtained using a graphite-monochromated Co Ka radiation (λ = 0.179 nm) on a D8
153 Discover GADDS system (Bruker, Madison, WI) operated at 40 kV and 35 mA.

154

155 ## RESULTS AND DISCUSSION

156 **Removal of Silver Ions by MoS_2 Dispersed in Aqueous Solution.** The ce-MoS_2 nanosheets
157 produced by chemically exfoliating bulk MoS_2 were primarily in monolayer form. As seen in the
158 AFM image (Figure S1a), the thickness profile of a representative MoS_2 nanosheet obtained by
159 step analysis had a clear step of ~1.2 nm, consistent with the reported thickness of around 1.2 nm
160 for monolayer MoS_2.[21] HRTEM images reveal that the lateral size of ce-MoS_2 nanosheets was

161 typically in the range of 200 to 500 nm (Figure S1b). The morphology of as-prepared ce-MoS_2
162 nanosheets is consistent with that reported previously.[21,33] Besides, ce-MoS_2 nanosheets were
163 dispersed well in water and aqueous solution due to their negatively charged surfaces,[32] thereby
164 maximizing the number of exposed sulfur atoms and thus potentially enhancing the removal of
165 heavy metal ions by adsorption.

166 The well-dispersed ce-MoS_2 nanosheets exhibited excellent Ag^+ removal performance in
167 terms of capacity, kinetics, and selectivity. Figure 1a plots the Ag^+ removal capacity by ce-MoS_2
168 nanosheets at room temperature (25 ◦C) as a function of Ag^+ equilibrium concentration (i.e., the
169 concentration of Ag^+ remaining in solution after the adsorption reached equilibrium). Ag^+ removal
170 increased promptly as Ag^+ equilibrium concentration increased initially and reached a plateau
171 immediately at a slightly higher equilibrium concentration (~ 20 ppm). Such experimental data are
172 fitted very well using the Langmuir adsorption model (Figure S2a),[37] which leads to a peak
173 removal capacity of 980 mg/g (Figure 1a) or 1.5 mol/mol, much higher than reported capacities (<
174 200 mg/g) of adsorbent materials such as carbon, zeolite, perlite, and resin.[38-41] The good fitting
175 implies an adsorption-based removal mechanism, consistent with findings from most of previous
176 reports on the use of MoS_2 nanosheets for heavy metal remediation.[15-20,24,25,27,28,42] The Ag^+
177 removal kinetics by ce-MoS_2 was studied using 40 ppm of Ag^+ added to 50 ppm of salt-free MoS_2
178 nanosheet suspension. It is observed in Figure S2b that that over 90% of the total Ag^+ was removed
179 within the first 15 min and over 99.5% removed (i.e., Ag^+ concentration was reduced to less than
180 0.2 ppm) after 3 h. The selectivity of ce-MoS_2 adsorbent was tested using 50 ppm of MoS_2
181 suspensions containing sodium nitrate with different ionic strengths ($NaNO_3$ concentrations up to
182 1 M), and it was found that 40 ppm of Ag^+ was removed almost completely after 1 day for each
183 MoS_2 suspension (Figure 1b).

184 Besides adsorption as the well-known removal mechanism of MoS_2 nanosheets, a new
185 mechanism that involves a reduction-oxidation (redox) reaction between ionic metal species and
186 ce-MoS_2 was discovered. To prove this mechanism, after Ag^+ removal tests, the Ag-containing
187 MoS_2 precipitates were isolated by centrifugation and characterized. As shown in Figure 1c, the
188 XRD patterns of the precipitates reveal the characteristic peaks of metallic Ag, implying a redox
189 reaction between Ag^+ and ce-MoS_2. Although bulk MoS_2 is capable of resisting ambient oxidation
190 attack due to its covalent bonding and lack of lone electron in S atoms,[29] MoS_2 nanosheets can be

oxidized (by oxygen) to molybdenum trioxide (MoO_3) in dry state[43,44] or soluble molybdate and sulfate/sulfite ions in aqueous solution.[36] Because Ag^+ (as well as other heavy metal ions such as Hg^{2+}, Au^{3+}, Pd^{2+}, and Pt^{2+}) is a mild oxidant, it may potentially oxidize MoS_2 nanosheets to soluble molybdate and sulfate/sulfite ions while reduce itself to metallic Ag(0) particle, as described by the following chemical equation:

$$18Ag^+ + MoS_2 + 12\,H_2O \rightarrow 18Ag(0) + MoO_4^{2-} + 2SO_4^{2-} + 24H^+ \quad (1)$$

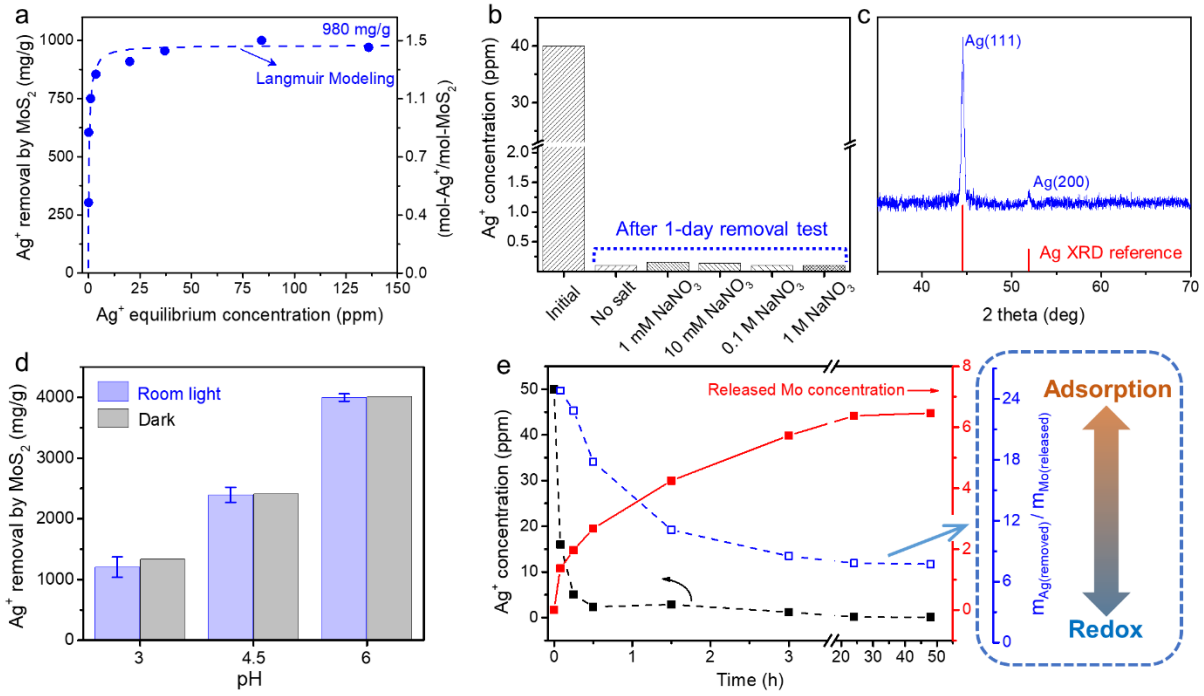

Figure 1. Ag^+ removal by ce-MoS_2 suspension. (a) Ag^+ removal at various equilibrium concentrations. (b) Selectivity of Ag^+ removal in solutions containing $NaNO_3$ with concentrations up to 1 M. (c) XRD patterns of isolated Ag-containing MoS_2 precipitates showing the characteristic peaks of metallic Ag. (d) Effects of pH and light conditions on Ag^+ removal. 30 ppm ce-MoS_2 suspension was added with excess Ag^+ in the acetate buffers (pH 3, 4.5) and MES buffer (pH 6). A control sample was covered with aluminum foil during the entire reaction to investigate the potential light effect. (e) Time-dependent Ag^+ removal and soluble Mo species release by a MoS_2 suspension (30 ppm) containing 50 ppm of Ag^+ at pH 6. The real-time mass ratio of removed Ag^+ to soluble Mo is used as an indicator for relative contributions of adsorption and redox reaction.

We studied factors (e.g., pH, light, Ag^+ concentration) that potentially influence the redox reaction between Ag^+ and ce-MoS_2. The pH condition was found to be critical for Ag^+ removal. At pH 3, 4.5, and 6, the Ag^+ removal capacity of ce-MoS_2 was approximately 1200, 2400, and

212 4000 mg/g (or 1.8, 3.6, and 6 mol/mol), respectively (Figure 1d), which are higher than that
213 obtained without buffer solutions (Figure 1a). Typically, the pH of Ag-MoS_2 suspensions in Figure
214 1a decreased from ~5 initially to ~3 after 1-d reaction because of proton release from the redox
215 reaction. As explained by Equation 1, higher pH accelerates the forward reaction for metallic Ag
216 deposition and hence enhances the removal capacity. Besides, light has been found to be an
217 indispensable catalyst in the redox reaction of Ag-thiol, the organic counterpart of Ag-S complex,
218 where Ag^+ is reduced to metallic particles by thiol groups.[45] However, the dark control test results
219 shown in Figure 1d reveal that the redox reaction between Ag^+ and MoS_2 can occur irrespective
220 of light conditions. We also investigated the effect of initial Ag^+ concentration on the redox
221 reaction, and found that the release of soluble molybdate after 1-day reaction increased almost
222 linearly with the increasing initial Ag^+ concentration (Figure S3), confirming a nearly
223 stoichiometric redox reaction that led to reductive removal of Ag^+ and concomitant release of
224 soluble MoO_4^{2-}.

225 In order to understand the relative contributions to silver removal by adsorption and redox
226 reaction, we conducted kinetics experiments in an anaerobic condition, which excluded the release
227 of soluble molybdate ions from ce-MoS_2 oxidation (by oxygen).[36] To continuously monitor the
228 change in the concentration of a mixture of Ag^+ and MoS_2 nanosheets, we took a vial of sample
229 and filtrated it through a 20-nm filter to remove any particulates, and then measured the
230 concentration of soluble species (Ag^+ and MoO_4^{2-}) in the filtrates. As shown in Figure 1e, the
231 concentration of soluble Ag^+ (bottom curve) decreased rapidly and reached 5 ppm (i.e., 90%
232 removal) in just 15 min, while the concentration of released molybdate ions (top curve) due to
233 Ag^+-induced MoS_2 oxidation increased relatively slowly. The mismatch between the kinetics of
234 Ag^+ removal and molybdate release is attributed to the difference between the rates of adsorption
235 and redox reaction. We calculated the mass ratio of the removed Ag^+ to the released MoO_4^{2-},
236 $m_{Ag(removed)}/m_{Mo(released)}$, as an indicator to differentiate the contributions of adsorption and redox
237 reaction. Since 1 mol MoS_2 can reduce a maximum of 18 mol Ag^+ while releasing 1 mol MoO_4^{2-}
238 and 2 mol SO_4^{2-}, the mass ratio of $m_{Ag(removed)}/m_{Mo(released)}$ is at most 20.2 if redox reaction were
239 the sole mechanism for removal. In fact, as shown by the blue (middle) curve in Figure 1e, the
240 mass ratio is ~24 within the first 15 min, implying Ag^+ removal mechanisms in the beginning
241 included both adsorption (the dominant one) and redox reaction. Then, the mass ratio decreases

242 gradually to as low as ~8 after a day and remains so afterwards, indicating that redox reaction
243 alone was the dominating mechanism during this period.

244 **Removal of Silver Ions by Layer-stacked MoS_2 Membrane.** A major challenge in using
245 suspended nanomaterials as adsorbents is the complete separation of nano-sized adsorbents from
246 water after use. For this reason, use of such nanomaterials in an aggregate form as opposed to
247 individual particulates for adsorption is appealing since the subsequent separation burden can be
248 alleviated significantly. On the other hand, however, the aggregation of nanomaterials possibly
249 reduces the overall surface area available for adsorption and hence poses a potential concern about
250 the removal efficiency. Therefore, it is important to evaluate and compare the Ag^+ removal
251 performances of MoS_2 nanosheets suspended in solution and layer-stacked as thin film membrane,
252 respectively.

253 Three MoS_2 membranes with different thicknesses (200, 400, and 600 nm, respectively)
254 were prepared on PES ultrafiltration substrates by a vacuum-assisted filtration method. After 1-
255 day incubation in Ag^+-excess solution at pH 6, a thicker MoS_2 membrane apparently recovered
256 more Ag particles on its surface than a thinner one (Figure 2a). However, the curves for Ag^+
257 removal over time, as determined by the concentration change of Ag^+ in solution and normalized
258 by the membrane mass, are similar for the three different membranes, with the 1-day removal
259 capacity of ~ 4000 mg/g closely matching that achieved by MoS_2 suspension (Figure 1d, pH 6),
260 suggesting the high removal capacity of suspended MoS_2 nanosheets can be retained by MoS_2
261 membranes (the mechanism will be discussed later).

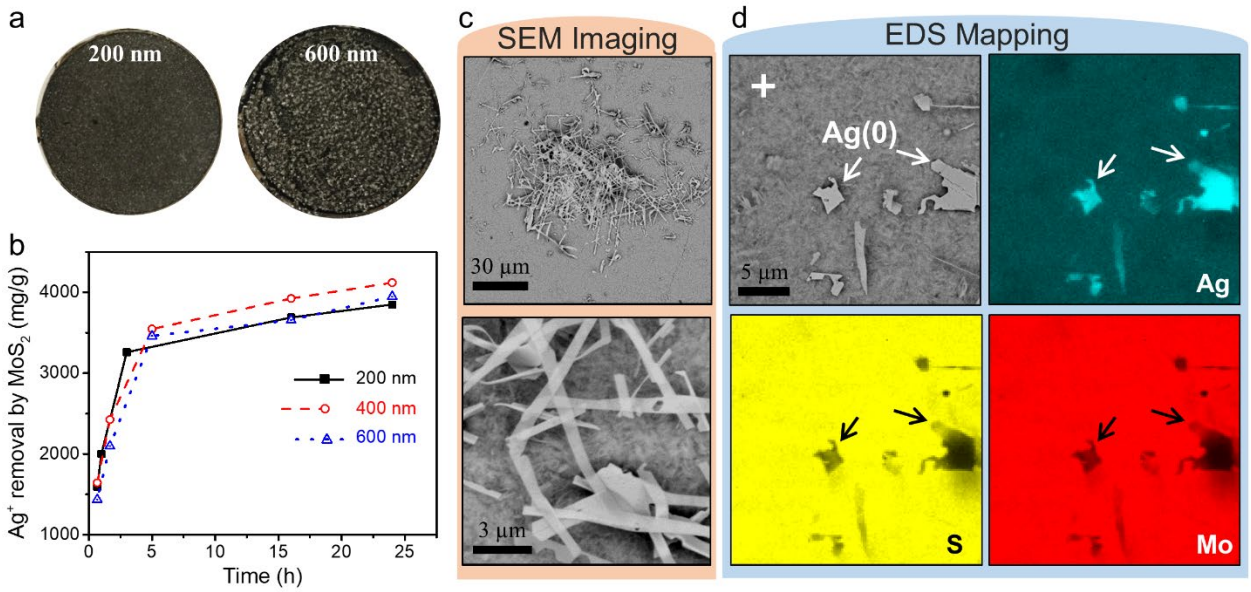

Figure 2. Removal and recovery of Ag^+ by layer-stacked MoS_2 membranes of different thicknesses: (a) Optical images of Ag particles deposited on membrane surfaces, and (b) real-time Ag^+ removal by MoS_2 membranes. Characterization of Ag particles on the 200-nm membrane: (c) SEM images with various magnifications revealing belt-like Ag particles, and (d) SEM and the corresponding EDS elemental mapping of a selected region of Ag-deposited MoS_2 membrane surface with reduced Ag(0) highlighted.

The SEM images (Figure 2c) show that the Ag particles deposited on the 200-nm MoS_2 membrane formed isolated clusters with a primarily belt-like structure, which was likely caused by the selective adsorption of released Mo and S species on opposite facets of a silver seed, leading to restricted growth on the passivated facets.[46] A selected surface region of the Ag-deposited MoS_2 membrane was further investigated with the EDS analysis of Ag, S, and Mo elements (Figure 2d). The elemental mapping shows that S and Mo elements were distributed evenly on the membrane surface except the areas shielded by Ag particles. In the EDS image for Ag element, the bright areas represent the metallic particles while the dark areas indicate the presence of a lower but detectable amount of silver element, which might be adsorbed Ag^+ on the MoS_2 membrane surface. Three particle-free regions were analyzed by EDS point elemental analysis, revealing the atomic concentrations of Ag, S, and Mo to be 27.8±0.4%, 48.5±0.5%, and 23.7±0.1%, respectively (Figure S4). The simultaneous existence of both adsorbed Ag^+ and Ag particles confirms that MoS_2 membranes also remove Ag^+ via two mechanisms — one is the adsorption of Ag^+ on individual MoS_2 surface and the other is the redox reaction that forms the segregated micrometer-sized metallic silver particles. Assuming that Ag detected in particle-free regions resulted solely from

284 adsorption, we calculated the adsorption capacity to be ~780 mg/g based on the atomic ratio of Ag
285 to S determined by the SEM elemental analysis (see calculation details in Figure S4). This is lower
286 than the theoretical maximum adsorption capacity of 1350 mg/g calculated by assuming that each
287 S atom in MoS_2 can absorb one Ag atom. With the total removal capacity of ~4000 mg/g (Figure
288 2b), the redox reaction should be the dominant mechanism for Ag^+ removal by ce-MoS_2
289 suspension and membranes.

290 **MoS_2 Phase Effect on Silver Ion Removal Mechanisms.** The adsorption and redox reaction
291 were found to be strongly affected by the specific phase (1T vs. 2H) of MoS_2. Unlike bulk MoS_2
292 in pure semiconducting 2H phase, the pristine ce-MoS_2 in this study consisted of both metallic 1T
293 and semiconducting 2H phases accounting for 60% and 40%, respectively, based on the XPS
294 spectra analysis (Figure 3a). After Ag^+ treatment (pH 6) of the 200-nm ce-MoS_2 membrane for 1
295 day, however, the peaks of Mo^{4+} 3d (Figure 3a) and S 2p (Figure S5) shift towards higher binding
296 energy by ~0.5 to 0.8 eV, and curve fitting implies a nearly complete degradation of 1T MoS_2,
297 leaving 2H as the sole phase. The preferential oxidation of the metastable 1T phase has been
298 associated with the conductive nanosheets that lead to a corrosion-type reaction.[36,47] We further
299 confirmed such a phase effect by demonstrating the drastically different Ag^+ removal behavior of
300 ue-MoS_2 nanosheet suspension, which can be similarly exfoliated from bulk material but its phase
301 composition is predominantly 2H. It was found that although ue-MoS_2 nanosheets were able to
302 remove Ag^+ with a moderate capacity of ~ 400 mg/g, no molybdate was released after 1-day
303 incubation in solutions of different Ag^+ concentrations up to 250 ppm (Figure S6). This
304 observation implies that redox reaction did not occur between Ag^+ and ue-MoS_2, consistent with
305 the stability of 2H phase against oxidation as reported in previous studies.[36,47] It is also worth
306 noting that there exist apparent, high peaks of oxidized Mo (Mo^{5+} and Mo^{6+})[48] at ~232 and 235 eV
307 in the XPS spectra of Ag^+-treated ce-MoS_2 membrane (Figure 3a), indicating the oxidation of Mo
308 atoms by Ag^+.

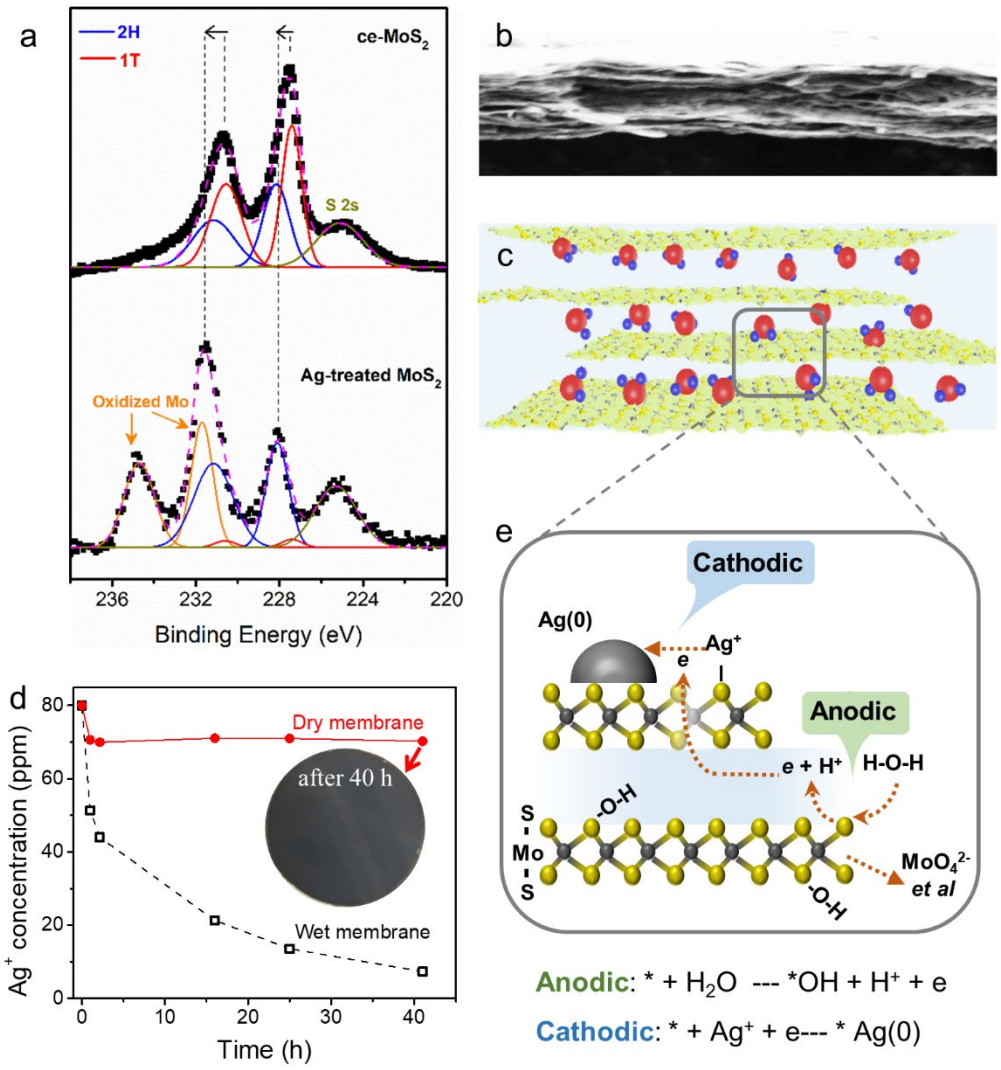

Figure 3. Mechanistic investigation of Ag^+ removal by ce-MoS_2 membrane. (a) XPS spectra of a pristine MoS_2 membrane and the membrane treated in Ag^+ solution at pH 6 for one day. (b) Cross-sectional SEM image of a typical MoS_2 membrane. (c) Schematic illustration of water-containing MoS_2 nanochannels. (d) Ag^+ removal behaviors of wet and dry MoS_2 membranes each incubated in Ag^+ solution with an initial concentration of 80 ppm. The dry MoS_2 membrane was made by drying a freshly prepared wet 200-nm MoS_2 membrane in vacuum oven at 60 °C for 3 h. (e) Proposed mechanism of redox reaction in a water-containing MoS_2 membrane.

The interlayer spacing of the MoS_2 membrane plays a critical role in its Ag^+ removal via the redox reaction mechanism. During the membrane preparation process, individual ce-MoS_2 nanosheets were stacked in parallel to form a well-aligned layered structure (Figure 3b). We have recently reported that water-containing MoS_2 nanochannels are able to maintain 1.2-nm interlayer spacing (equivalently 0.9-nm free spacing) through the balance between hydration force and van

323 der Waals force.[35,49] The water molecules confined in such nanochannels (Figure 3c) are critical
324 for MoS_2 to remove heavy metal ions. This is because, after a MoS_2 membrane is dried completely,
325 its interlayer spacing decreases to 0.62 nm (or merely 0.3-nm free spacing),[35] which prevents water
326 and metal ions from intercalating and accessing the interior sulfur atoms. Without the necessary
327 reactant water molecules, the dry MoS_2 membrane cannot effectively reduce Ag^+. As shown by
328 the inset in Figure 3d, Ag^+ was unable to be reduced effectively by a dry MoS_2 membrane and
329 hence no Ag particles were formed on membrane surface.

330 The corrosion-type reaction mechanism of individual 1T MoS_2 nanosheets[47] is also
331 applicable to MoS_2 nanosheets restacked as thin film membrane. As illustrated in Figure 3e,
332 conductive 1T phase serves as both an anode and a cathode.[47,49] Electrons are donated from 1T
333 MoS_2 at one site in an anodic reaction, and transferred via conductive 1T and/or water-containing
334 nanochannels[49] to another site where Ag^+ is reduced to metallic particle. In the oxidation process,
335 water molecules release protons and gradually add (in the form of OH adsorbates) onto S and Mo
336 atoms, which are eventually released as soluble species. The Ag particles are primarily reduced on
337 the membrane surface, where the highest concentration of Ag^+ is present. Ag^+ can diffuse to the
338 membrane interior and form particles there, as evidenced by the more porous membrane structure
339 with thickness enlarged from ~ 600 nm to 10 μm (Figure S7a) apparently due to an increase in
340 interlayer spacing as Ag particles were formed inside. In addition, the presence of Ag is also
341 supported by the EDS mapping of the membrane cross-sectional regions (Figure S7b).

342 **Removal of Silver Ions by MoS_2 Membrane Filtration.** We also tested the heavy metal removal
343 capability of MoS_2 membrane in continuous filtration mode, where feed solutions with Ag^+
344 concentrations of 2 ppm and 20 ppm were each filtrated through a 200-nm MoS_2 membrane under
345 a pressure of 20 psi (~1.4 bar). It is observed in Figure S8 that the MoS_2 membrane was able to
346 effectively remove Ag ions from the 2-ppm feed solution, as the Ag^+ concentration of the filtrate
347 solution was less than 0.01 ppm. In comparison, for the 20-ppm feed solution, the removal
348 efficiency by the MoS_2 membrane was ~ 99 % (0.2 ppm in the filtrate solution) in the beginning
349 but showed a generally decreasing trend as more feed solution was filtrated through the membrane.
350 Such a decrease in removal efficiency was caused by membrane oxidative degradation (Figure
351 S8b) due to the redox reaction between the Ag^+-MoS_2 pair, which shortened the time of contact
352 between Ag^+ and MoS_2 membrane. The membrane oxidative degradation was also evidenced by

353 the increased water flux (Figure S8c) and detected soluble Mo species (MoO_4^{2-}) in the filtrate of
354 the 200-nm MoS_2 membrane (Figure S8d).

355 **Potential for Removal of Other Metal Ions.** 2D MoS_2 nanosheets have been extensively
356 explored for their capability of removing heavy metal ions by adsorption. The unveiling of redox
357 reaction as a new removal mechanism opens up new opportunities for 2D MoS_2 in heavy metal
358 remediation. Depending on their relative redox potentials, heavy metal ions can be removed
359 primarily by either adsorption or redox reaction. The redox potential of MoO_4^{2-} and SO_4^{2-}/MoS_2
360 pair has been reported to be 0.429 V,[36,50] and consequently MoS_2 is able to reduce heavy metal
361 ions in the redox couples with higher redox potentials, including Au^{3+}, Hg^{2+} as well as other heavy
362 metal ions in the "redox and adsorptive removal" category (Figure 4). For those heavy metal ions
363 that MoS_2 is unable to reduce, they can be potentially eliminated by "adsorptive removal" via
364 Lewis soft-soft interactions. In addition, MoS_2 nanosheets are capable of quenching reactive
365 oxygen species (ROSs), giving rise to antioxidant applications such as conformal coating that can
366 mitigate ROS production and toxicity.

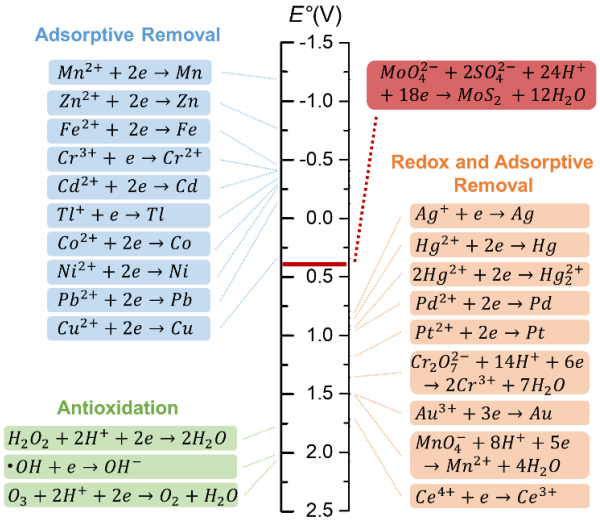

367

368 **Figure 4.** Comparison of reduction potentials of MoO_4^{2-} and SO_4^{2-}/MoS_2 with other pairs common in heavy
369 metal remediation and antioxidation.
370
371 We used Hg^{2+} and Au^{3+} as examples to further demonstrate the removal capability of MoS_2
372 membranes. As shown in Figure S9a, both the oxidative dissolution of MoS_2 in the presence of
373 Hg^{2+} and the color change of membrane surface indicate a redox reaction between Hg^{2+} and MoS_2.
374 The redox reaction between Au^{3+} and MoS_2 is evidenced by the formation of yellowish gold film

375 on membrane surface (Figure S9b). After 2 days, 5 mg Au^{3+} was removed completely by the MoS_2
376 membrane (2 mg), amounting to a removal capacity of 2500 mg/g. The lower Au^{3+}removal
377 capacity as compared to Ag^+ removal capacity (~4000 mg/g) by MoS_2 is attributed to the need of
378 more electrons in the redox reaction of Au^{3+}.

379
380
381 **Environmental Implications.** The redox reactions between certain heavy metal ions and MoS_2
382 nanosheets have significant implications for environmental remediation. In the present study, we
383 have demonstrated that the metallic 1T phase ce-MoS_2 nanosheet is conductive and capable of
384 removing certain heavy metal ions through a corrosion-type chemical reaction, thereby unveiling
385 a new mechanism besides the well-known adsorption for the removal of heavy metal ions by ce-
386 MoS_2. Considering the ubiquitous existence of 1T phase in most synthetic MoS_2 nanosheets,[21,23,30]
387 we believe that most MoS_2 nanomaterials could remove heavy metal ions via redox reaction, at
388 least to some extent. Thus, it is beneficial to consider the redox reaction as a removal mechanism
389 when using TMDs as adsorbents. Recognizing this redox chemistry, we have engineered ce-MoS_2
390 nanosheets into layer-stacked membranes, which offer several remarkable advantages in precious
391 metal recovery compared to conventional adsorbents. First, the exposed sulfur atoms on membrane
392 surface have high affinity to heavy metal ions, which typically are Lewis soft acids, and thus
393 increase the removal kinetics. Second, the MoS_2 membrane is colloidally stable against
394 redispersion because of the strong van der Waals force,[35] and capable of utilizing the interior MoS_2
395 by undergoing a corrosion-type reaction through the conductive structure. Lastly, the oxidation
396 products are primarily soluble, non-toxic molybdate and sulfur species, which do not passivate the
397 membrane surface for not forming any insulating oxide layers.

398

399

400

401 **ASSOCIATED CONTENT**

402 **Supporting Information**. AFM and HRTEM images of as-prepared MoS_2 nanosheets (Figure
403 S1); Langmuir adsorption model fitting and adsorption kinetics curve for Ag removal (Figure S2);
404 Effects of initial Ag^+ concentration on the release of soluble molybdate ions (Figure S3); Atomic

concentrations of three sample particle-free regions on a Ag-deposited MoS_2 membrane surface (Figure S4); XPS spectra (S 2p) of pristine and Ag-treated MoS_2 membrane (Figure S5); Removal capacities of ue-MoS_2 nanosheets and the corresponding soluble Mo concentrations using solutions with different initial Ag^+ concentrations (Figure S6); Cross-sectional SEM and EDS elemental mapping images of a Ag-deposited MoS_2 membrane (Figure S7); Water flux as well as Ag^+ and Mo concentrations in filtrate by MoS_2 membranes (Figure S8); Removal of Hg^{2+} and Au^{3+} by MoS_2 membranes (Figure S9). (PDF)

ACKNOWLEDGEMENT

The material is based upon work supported by the U.S. National Science Foundation under award nos. CBET-1565452 and CBET-1706059. Work at the Molecular Foundry was supported by the Office of Science, Office of Basic Energy Sciences, of the U.S. Department of Energy under contract no. DE-AC02-05CH11231. However, the opinions expressed herein are those of the authors and do not necessarily reflect those of the sponsors.

REFERENCE

(1) Montgomery, M. A.; Elimelech, M., Water and sanitation in developing countries: including health in the equation. *Environ. Sci. Technol.* **2007,** *41* (1), 17-24.

(2) Fu, F.; Wang, Q., Removal of heavy metal ions from wastewaters: a review. *J. Environ. Manage.* **2011,** *92* (3), 407-418.

(3) Kobya, M.; Demirbas, E.; Senturk, E.; Ince, M., Adsorption of heavy metal ions from aqueous solutions by activated carbon prepared from apricot stone. *Bioresour. Technol.* **2005,** *96* (13), 1518-1521.

(4) Celis, R.; Hermosin, M. C.; Cornejo, J., Heavy metal adsorption by functionalized clays. *Environ. Sci. Technol.* **2000,** *34* (21), 4593-4599.

(5) Liu, P.; Borrell, P. F.; Božič, M.; Kokol, V.; Oksman, K.; Mathew, A. P., Nanocelluloses and their phosphorylated derivatives for selective adsorption of Ag^{+}, Cu^{2+} and Fe^{3+} from industrial effluents. *J. Hazard. Mater.* **2015,** *294*, 177-185.

(6) Zhao, G.; Li, J.; Ren, X.; Chen, C.; Wang, X., Few-layered graphene oxide nanosheets as superior sorbents for heavy metal ion pollution management. *Environ. Sci. Technol.* **2011,** *45* (24), 10454-10462.

(7) Ahluwalia, S. S.; Goyal, D., Microbial and plant derived biomass for removal of heavy metals from wastewater. *Bioresour. Technol.* **2007,** *98* (12), 2243-2257.

(8) Li, Y.-H.; Ding, J.; Luan, Z.; Di, Z.; Zhu, Y.; Xu, C.; Wu, D.; Wei, B., Competitive adsorption of Pb^{2+}, Cu^{2+} and Cd^{2+} ions from aqueous solutions by multiwalled carbon nanotubes. *Carbon* **2003,** *41* (14), 2787-2792.

(9) Lasko, C. L.; Hurst, M. P., An investigation into the use of chitosan for the removal of soluble silver from industrial wastewater. *Environ. Sci. Technol.* **1999,** *33* (20), 3622-3626.

(10) Manos, M. J.; Kanatzidis, M. G., Metal sulfide ion exchangers: superior sorbents for the capture of toxic and nuclear waste-related metal ions. *Chemical Science* **2016,** *7* (8), 4804-4824.

(11) Ma, L.; Wang, Q.; Islam, S. M.; Liu, Y.; Ma, S.; Kanatzidis, M. G., Highly selective and efficient removal of heavy metals by layered double hydroxide intercalated with the MoS_4^{2-} ion. *J. Am. Chem. Soc.* **2016,** *138* (8), 2858-2866.

(12) Zhang, W.; Shi, S.; Zhu, W.; Yang, C.; Li, S.; Liu, X.; Hu, N.; Huang, L.; Wang, R.; Suo, Y., In-situ fixation of all-inorganic Mo–Fe–S clusters for the highly selective removal of lead(II). *ACS Appl. Mater. Interfaces* **2017,** *9* (38), 32720-32726.

(13) Shin, Y.; Fryxell, G. E.; Um, W.; Parker, K.; Mattigod, S. V.; Skaggs, R., Sulfur‐functionalized mesoporous carbon. *Adv. Funct. Mater.* **2007,** *17* (15), 2897-2901.

(14) Wang, Z.; Mi, B., Environmental applications of 2D molybdenum disulfide (MoS_2) nanosheets. *Environ. Sci. Technol.* **2017,** *51* (15), 8229-8244.

(15) Jia, F.; Zhang, X.; Song, S., AFM study on the adsorption of Hg^{2+} on natural molybdenum disulfide in aqueous solutions. *PCCP* **2017,** *19* (5), 3837-3844.

(16) Jia, F.; Wang, Q.; Wu, J.; Li, Y.; Song, S., Two-dimensional molybdenum disulfide as a superb adsorbent for removing Hg^{2+} from water. *ACS Sustain. Chem. Eng.* **2017,** *5* (8), 7410-7419.

(17) Zhi, L.; Zuo, W.; Chen, F.; Wang, B., 3D MoS_2 composition aerogel as chemosensors and adsorbents for colorimetric detection and high-capacity adsorption of Hg^{2+}. *ACS Sustain. Chem. Eng.* **2016,** *4* (6), 3398-3408.

(18) Ai, K.; Ruan, C.; Shen, M.; Lu, L., MoS_2 nanosheets with widened interlayer spacing for high‐efficiency removal of mercury in aquatic systems. *Adv. Funct. Mater.* **2016,** *26* (30), 5542-5549.

(19) Zhao, H.; Yang, G.; Gao, X.; Pang, C. H.; Kingman, S. W.; Wu, T., Hg0 capture over CoMoS/γ-Al_2O_3 with MoS_2 nanosheets at low temperatures. *Environ. Sci. Technol.* **2016,** *50* (2), 1056-1064.
(20) Aghagoli, M. J.; Shemirani, F., Hybrid nanosheets composed of molybdenum disulfide and reduced graphene oxide for enhanced solid phase extraction of Pb(II) and Ni(II). *Microchim. Acta* **2017,** *184* (1), 237-244.
(21) Eda, G.; Yamaguchi, H.; Voiry, D.; Fujita, T.; Chen, M.; Chhowalla, M., Photoluminescence from chemically exfoliated MoS_2. *Nano Lett.* **2011,** *11* (12), 5111-5116.
(22) Smith, R. J.; King, P. J.; Lotya, M.; Wirtz, C.; Khan, U.; De, S.; O'Neill, A.; Duesberg, G. S.; Grunlan, J. C.; Moriarty, G., Large‐scale exfoliation of inorganic layered compounds in aqueous surfactant solutions. *Adv. Mater.* **2011,** *23* (34), 3944-3948.
(23) Liu, Q.; Li, X.; He, Q.; Khalil, A.; Liu, D.; Xiang, T.; Wu, X.; Song, L., Gram‐scale aqueous synthesis of stable few-layered 1T‐MoS_2: applications for visible‐light‐driven photocatalytic hydrogen evolution. *Small* **2015,** *11* (41), 5556-5564.
(24) Wang, J.; Zhang, W.; Yue, X.; Yang, Q.; Liu, F.; Wang, Y.; Zhang, D.; Li, Z.; Wang, J., One-pot synthesis of multifunctional magnetic ferrite–MoS_2–carbon dot nanohybrid adsorbent for efficient Pb(II) removal. *J. Mater. Chem. A* **2016,** *4* (10), 3893-3900.
(25) Tong, S.; Deng, H.; Wang, L.; Huang, T.; Liu, S.; Wang, J., Multi-functional nanohybrid of ultrathin molybdenum disulfide nanosheets decorated with cerium oxide nanoparticles for preferential uptake of lead(II) ions. *Chem. Eng. J.* **2018,** *335*, 22-31.
(26) Liu, C.; Jia, F.; Wang, Q.; Yang, B.; Song, S., Two-dimensional molybdenum disulfide as adsorbent for high-efficient Pb(II) removal from water. *Appl. Mater. Today* **2017,** *9*, 220-228.
(27) Wang, J.; Wang, P.; Wang, H.; Dong, J.; Chen, W.; Wang, X.; Wang, S.; Hayat, T.; Alsaedi, A.; Wang, X., Preparation of molybdenum disulfide coated Mg/Al layered double hydroxide composites for efficient removal of chromium(VI). *ACS Sustain. Chem. Eng.* **2017,** *5* (8), 7165–7174.
(28) Aghagoli, M. J.; Beyki, M. H.; Shemirani, F., Application of dahlia-like molybdenum disulfide nanosheets for solid phase extraction of Co(II) in vegetable and water samples. *Food Chem.* **2017,** *223*, 8-15.
(29) Chhowalla, M.; Shin, H. S.; Eda, G.; Li, L.-J.; Loh, K. P.; Zhang, H., The chemistry of two-dimensional layered transition metal dichalcogenide nanosheets. *Nat. Chem.* **2013,** *5* (4), 263-275.
(30) Shi, Z.-T.; Kang, W.; Xu, J.; Sun, Y.-W.; Jiang, M.; Ng, T.-W.; Xue, H.-T.; Denis, Y.; Zhang, W.; Lee, C.-S., Hierarchical nanotubes assembled from MoS_2-carbon monolayer sandwiched superstructure nanosheets for high-performance sodium ion batteries. *Nano Energy* **2016,** *22*, 27-37.
(31) Joensen, P.; Crozier, E.; Alberding, N.; Frindt, R., A study of single-layer and restacked MoS_2 by X-ray diffraction and X-ray absorption spectroscopy. *J. Phys. C: Solid State Phys.* **1987,** *20* (26), 4043.
(32) Heising, J.; Kanatzidis, M. G., Exfoliated and restacked MoS_2 and WS_2: Ionic or neutral species? Encapsulation and ordering of hard electropositive cations. *J. Am. Chem. Soc.* **1999,** *121* (50), 11720-11732.
(33) Chou, S. S.; De, M.; Kim, J.; Byun, S.; Dykstra, C.; Yu, J.; Huang, J.; Dravid, V. P., Ligand conjugation of chemically exfoliated MoS_2. *J. Am. Chem. Soc.* **2013,** *135* (12), 4584-4587.
(34) Deng, M.; Kwac, K.; Li, M.; Jung, Y.; Park, H. G., Stability, molecular sieving, and ion diffusion selectivity of a lamellar membrane from two-dimensional molybdenum disulfide. *Nano Lett.* **2017,** *17* (4), 2342–2348.

(35) Wang, Z.; Tu, Q.; Zheng, S.; Urban, J. J.; Li, S.; Mi, B., Understanding the aqueous stability and filtration capability of MoS_2 membranes. *Nano Lett.* **2017,** *17* (12), 7289-7298.
(36) Wang, Z.; von dem Bussche, A.; Qiu, Y.; Valentin, T. M.; Gion, K.; Kane, A. B.; Hurt, R. H., Chemical dissolution pathways of MoS_2 nanosheets in biological and environmental media. *Environ. Sci. Technol.* **2016,** *50* (13), 7208–7217.
(37) Foo, K. Y.; Hameed, B. H., Insights into the modeling of adsorption isotherm systems. *Chem. Eng. J.* **2010,** *156* (1), 2-10.
(38) Wang, S.; Li, H.; Chen, X.; Yang, M.; Qi, Y., Selective adsorption of silver ions from aqueous solution using polystyrene-supported trimercaptotriazine resin. *J. Environ. Sci.* **2012,** *24* (12), 2166-2172.
(39) Song, X.; Gunawan, P.; Jiang, R.; Leong, S. S. J.; Wang, K.; Xu, R., Surface activated carbon nanospheres for fast adsorption of silver ions from aqueous solutions. *J. Hazard. Mater.* **2011,** *194*, 162-168.
(40) Ghassabzadeh, H.; Mohadespour, A.; Torab-Mostaedi, M.; Zaheri, P.; Maragheh, M. G.; Taheri, H., Adsorption of Ag, Cu and Hg from aqueous solutions using expanded perlite. *J. Hazard. Mater.* **2010,** *177* (1), 950-955.
(41) Akgül, M.; Karabakan, A.; Acar, O.; Yürüm, Y., Removal of silver (I) from aqueous solutions with clinoptilolite. *Microporous Mesoporous Mater.* **2006,** *94* (1), 99-104.
(42) Subrahmanyam, K. S.; Malliakas, C. D.; Sarma, D.; Armatas, G. S.; Wu, J.; Kanatzidis, M. G., Ion-exchangeable molybdenum sulfide porous chalcogel: Gas adsorption and capture of iodine and mercury. *J. Am. Chem. Soc.* **2015,** *137* (43), 13943-13948.
(43) Gao, J.; Li, B.; Tan, J.; Chow, P.; Lu, T.-M.; Koratkar, N., Aging of transition metal dichalcogenide monolayers. *ACS Nano* **2016,** *10* (2), 2628-2635.
(44) Yamamoto, M.; Einstein, T. L.; Fuhrer, M. S.; Cullen, W. G., Anisotropic etching of atomically thin MoS_2. *J. Phys. Chem. C* **2013,** *117* (48), 25643-25649.
(45) Liu, J.; Wang, Z.; Liu, F. D.; Kane, A. B.; Hurt, R. H., Chemical transformations of nanosilver in biological environments. *ACS Nano* **2012,** *6* (11), 9887-9899.
(46) Huang, T.-K.; Cheng, T.-H.; Yen, M.-Y.; Hsiao, W.-H.; Wang, L.-S.; Chen, F.-R.; Kai, J.-J.; Lee, C.-Y.; Chiu, H.-T., Growth of Cu nanobelt and Ag belt-like materials by surfactant-assisted galvanic reductions. *Langmuir* **2007,** *23* (10), 5722-5726.
(47) Wang, Z.; Zhang, Y.-J.; Liu, M.; Peterson, A.; Hurt, R. H., Oxidation suppression during hydrothermal phase reversion allows synthesis of monolayer semiconducting MoS_2 in stable aqueous suspension. *Nanoscale* **2017,** *9* (17), 5398-5403.
(48) Lee, Y.-J.; Barrera, D.; Luo, K.; Hsu, J. W., In situ chemical oxidation of ultrasmall MoO_x nanoparticles in suspensions. *J. Nanotechnol.* **2012,** *2012*, 195761.
(49) Geng, X.; Zhang, Y.; Han, Y.; Li, J.; Yang, L.; Benamara, M.; Chen, L.; Zhu, H., Two-dimensional water-coupled metallic MoS_2 with nanochannels for ultrafast supercapacitors. *Nano Lett.* **2017,** *17* (3), 1825-1832.
(50) Wang, Z.; Zhu, W.; Qiu, Y.; Yi, X.; von dem Bussche, A.; Kane, A.; Gao, H.; Koski, K.; Hurt, R., Biological and environmental interactions of emerging two-dimensional nanomaterials. *Chem. Soc. Rev.* **2016,** *45* (6), 1750-1780.